Stochastic discrete event simulation of germinal center reactions

Marc Thilo Figge*
Centre for Theoretical Physics, University of Groningen, Nijenborgh 4, 9747 AG Groningen, The Netherlands
(Received 7 October 2004; published 24 May 2005)

We introduce a generic reaction-diffusion model for germinal center reactions and perform numerical simulations within a stochastic discrete event approach. In contrast to the frequently used deterministic continuum approach, each single reaction event is monitored in space and time in order to simulate the correct time evolution of this complex biological system. Germinal centers play an important role in the immune system by performing a reaction that aims at improving the affinity between antibodies and antigens. Our model captures experimentally observed features of this reaction, such as the development of the remarkable germinal center morphology and the maturation of antibody-antigen affinity in the course of time. We model affinity maturation within a simple affinity class picture and study it as a function of the distance between the initial antibody-antigen affinity and the highest possible affinity. The model reveals that this mutation distance may be responsible for the experimentally observed all-or-none behavior of germinal centers; i.e., they generate either mainly output cells of high affinity or no high-affinity output cells at all. Furthermore, the exact simulation of the system dynamics allows us to study the hypothesis of cell recycling in germinal centers as a mechanism for affinity optimization. A comparison of three possible recycling pathways indicates that affinity maturation is optimized by a recycling pathway that has previously not been taken into account in deterministic continuum models.

DOI: 10.1103/PhysRevE.71.051907 PACS number(s): 87.18.−h, 05.45.−a, 05.10.Ln

I. INTRODUCTION

Germinal centers play an important role in the response of the immune system to invading pathogenic organisms [1,2]. They appear in lymphoid tissue on antigenic stimulation and start a reaction that aims to improve the recognition of antigens by antibodies. The latter are soluble forms of specific B cell receptors. During the process of affinity maturation, the B cells undergo clonal amplifications, receptor hypermutations, and selection for highly specific receptors. This reaction takes place in the presence of follicular dendritic cells that provide antigen, and under the control of T cells that help with the differentiation of B cells into output cells.

From a theoretical point of view, germinal centers represent a typical example of a highly dynamic biological system, in which various coupled reaction processes occur on different characteristic time scales in a spatially compartmentalized microenvironment. Modeling such a complex system can be done in various conceptual ways that differ in the level of accuracy. In a deterministic continuum approach, reaction processes are considered as if taking place in a well-stirred mixture of cells and obeying the law of mass action. The cell concentrations are described by a set of coupled ordinary differential equations and change deterministically and continuously in time. This approach has the great computational advantage that only one single variable is required per cell type. It is often used to model biological systems and has also been applied to describe aspects of germinal center reactions [3–8].

The deterministic continuum approach is strictly speaking only applicable to systems where all cell types occur in large numbers, so that local inhomogeneities related to the discrete nature of cells and stochastic fluctuations in reaction processes can be neglected. Taking into account fluctuations in reaction processes may be realized by writing the rate equations in terms of a set of coupled Langevin equations for the average cell concentrations. This is a stochastic continuum approach, where one still deals with average cell concentrations; however, these are now changing in a more realistic, stochastic way. In the context of germinal centers this type of approach has, for example, been applied to account for randomness in the selection of specific B cell receptors [9,10].

On a microscopic scale cells have to be considered as discrete entities that undergo discrete events by diffusing through the system and reacting stochastically with each other. A stochastic discrete event approach takes this into account by monitoring the course of events for each single cell of the system in space and time. This approach is most conveniently formulated in terms of a master equation. The master equation determines the time evolution of the probability distribution to find the system in a particular state at a particular time. Numerical simulations of the system's time evolution have to be performed in such a way that the underlying probability distribution is a solution of the master equation. This does demand large computer resources, but is the only appropriate way to simulate highly dynamic biological systems where various cell types may be present in small numbers only. The stochastic discrete event approach has been applied to simulate spatial aspects of germinal centers, such as their morphology and the affinity maturation [11–13].

In this paper we introduce a generic reaction-diffusion model for germinal center reactions and perform stochastic discrete event simulations. In doing this, we apply the philosophy that *everything should be made as simple as possible, but not simpler* [14]. In other words, on the one hand

*Electronic address: m.t.figge@phys.rug.nl

our model will be as simple as possible, while on the other hand we will apply exact simulation methods in an efficient way. These methods have previously been proven to be powerful in simulating chemical reactions in solutions [15–17] and on surfaces [18]. We will discuss our simulation results with respect to the germinal center morphology and affinity maturation in the light of experimental observations. In particular, we will show that the all-or-none behavior of germinal centers can be related to the size of the maximal mutation distance within a simple affinity class picture. We find that, if the maximal mutation distance between the germline affinity class and the class of highest affinity exceeds a critical value, the germinal center reaction is not successful generating only output cells of low affinity. Furthermore, we investigate the impact of hypothetic centrocyte-centroblast recycling mechanisms on the affinity maturation. We compare the case of centrocytes that recycle only after having received both survival signals from interactions with antigen and with T cells, with the case of centrocytes that are allowed to recycle already after having received the first survival signal from interaction with antigen. The results of our numerical simulations indicate that only the latter recycling mechanism yields optimized affinity maturation and that recycling mechanisms in general are paid for by an eventually significant decrease in the number of output cells.

The paper is organized as follows: We describe the role of germinal centers in the humoral immune response in Sec. II and introduce in Sec. III our microscopic reaction-diffusion model. Next, in Sec. IV, we explain how to perform in an efficient way discrete event simulations of reaction-diffusion systems with space- and time-dependent reaction rates. The simulation results of numerical germinal center reactions with respect to morphology, affinity maturation, and recycling are presented and discussed in Sec. V. Finally, in Sec. VI, we summarize and conclude this paper.

II. GERMINAL CENTER REACTION

This section provides a brief description of germinal center reactions, where we restrict our considerations to generally accepted mechanisms [1,2].

The immune system defends living organisms in a humoral immune response against pathogenic invaders such as bacteria and viruses. This is achieved by the binding of antibodies to these antigens. The binding is specific and capable of discriminating between self and nonself in order to avoid autoimmune reactions [19,20]. An antibody-antigen complex acts as a signal for particular types of immune cells—e.g., macrophages—that engulf and kill the invader. It is obvious that the success of this mechanism depends on the ability of the antibody to bind the antigen and it has been observed that the affinity between antibody and antigen can increase in the course of time. This phenomenon is called affinity maturation and involves the generation of mutations in the genes that code for the antibody variable region, followed by an affinity based selection procedure.

Affinity maturation takes place in germinal centers, which form in secondary lymphoid tissue such as lymph nodes, tonsils, and the spleen. A germinal center is a lymph follicle which evolves into a highly dynamic and spatially compartmentalized microenvironment, which is schematically shown in Fig. 1. The germinal center is developed after the recognition of antigens by surface antibodies of B cells. The B cells play a key role in the germinal center reaction, which is started by only a few activated B cells that divide and fill the whole germinal center within about three days. These proliferating B cells are referred to as centroblasts, which are special in the sense that their surface antibodies are downregulated. After the first 3 days centroblasts differentiate into centrocytes, which are germinal center B cells that do not proliferate but do express surface antibodies. Starting from about this time centroblasts undergo intense hypermutation while they continue to proliferate and differentiate into centrocytes. As a result a repertoire of centrocytes with different types of surface antibodies is obtained. How exactly centroblast proliferation and differentiation is regulated is still unclear today.

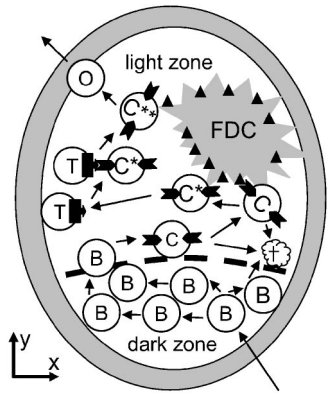

FIG. 1. Schematic representation of a germinal center reaction several days after initiation. The dark zone contains centroblasts (B) that proliferate and differentiate into centrocytes (C). Centrocytes may experience apoptosis (†) or bind with their surface antibodies to antigens (triangles) that are located at follicular dendritic cells (FDC) in the light zone. Activated centrocytes ($C^{\star}$) can bind to T cells (T) to obtain a second survival signal. These centrocytes ($C^{\star\star}$) can then differentiate into output cells (O). See the text for details.

In the course of the germinal center reaction two compartments develop, which are called the light zone and the dark zone (see Fig. 1). The mechanism that drives their appearance is also still unresolved today; however, it is observed that the dark zone contains predominantly proliferating centroblasts, while the light zone contains beside centrocytes various other cell types. Of great importance are antigen-specific T cells and follicular dendritic cells in the light zone. The latter bind antigen and present it to the surface antibodies of centrocytes. If centrocytes bind to antigen on follicular dendritic cells, they receive a survival signal which rescues them from apoptosis—i.e., from cell death which would otherwise naturally occur. This is a selection process for centrocytes based on their antibody-antigen affinity.

On separating again from the follicular dendritic cell the centrocyte takes up some antigen portion. This centrocyte eventually meets an antigen-specific T cell in the light zone and receives a second survival signal on presenting the antigen portion. It is commonly believed that this signal is re-

quired to ensure self-nonself discrimination, since under normal circumstances T cells effectively recognize portions of foreign molecules only. In addition, T cells are believed to play a mediating role in the differentiation of centrocytes into output cells. The output cells are either plasma or memory B cells. They are specific to antigen with an affinity that is usually significantly higher than that of the B cells by which the germinal center reaction was started. In particular, memory B cells are long-living cells that can respond quickly upon a second exposure to the same antigen, while plasma cells are able to secrete large amounts of antibodies which bind antigens making them easy prey to be killed by macrophages.

The end of the germinal center reaction is reached after about three weeks and is characterized by centroblasts ceasing to proliferate and disappearing together with centrocytes.

III. REACTION-DIFFUSION MODEL

We introduce a microscopic reaction-diffusion model for a germinal center on a d-dimensional lattice with N sites. Each site can either be occupied by a cell or be empty, while reaction processes can either occur on site or involve two nearest-neighbor sites. We will first consider basic reaction processes and then discuss in separate sections centroblast hypermutation, reaction regulation, and centrocyte-centroblast recycling, since these aspects deserve some more attention. We will use the following symbols: A for an antigen presenting site located on a follicular dendritic cell, B for a centroblast, C ($C^\star$, $C^{\star\star}$) for a centrocyte (having received, respectively, one or two survival signals), T for a T cell, O for an output cell—i.e., we do not explicitly distinguish plasma and memory B cells—and $\emptyset$ for an empty site.

A. Basic reaction processes in germinal centers

The model accounts for reactions that capture the main processes during a germinal center reaction as described in Sec. II. This includes the proliferation of centroblasts,

$$B + \emptyset \to B + B \text{ with rate } r(B\emptyset, BB), \tag{1}$$

and their differentiation into centrocytes,

$$B \to C \text{ with rate } r(B, C). \tag{2}$$

Centrocytes receive their first survival signal from the interaction with antigens presented at sites on follicular dendritic cells,

$$C + A \to C^\star + A \text{ with rate } r(CA, C^\star A). \tag{3}$$

The second survival signal for centrocytes comes from interaction with T cells,

$$C^\star + T \to C^{\star\star} + T \text{ with rate } r(C^\star T, C^{\star\star} T). \tag{4}$$

The T cells have migrated into the germinal center from particular zones outside the germinal center, which we simply model by the reaction process

$$\emptyset \to T \text{ with rate } r(\emptyset, T) \tag{5}$$

inside the germinal center. Centrocytes that have received both survival signals differentiate into output cells,

$$C^{\star\star} \to O \text{ with rate } r(C^{\star\star}, O), \tag{6}$$

where O denotes both plasma and memory B cells.

Furthermore, each cell in the germinal center can move by diffusion which is represented by a jump process from its site to an unoccupied neighbor site,

$$X + \emptyset \to \emptyset + X \text{ with rate } r(X\emptyset, \emptyset X), \tag{7}$$

where $X = B$, C, $C^\star$, $C^{\star\star}$, T, or O. The positions of antigen presenting sites on follicular dendritic cells, A, are kept fixed throughout the simulation.

Finally, the reaction

$$X \to \emptyset \text{ with rate } r(X, \emptyset) \tag{8}$$

describes apoptosis for cells $X = T$, B, and C that are removed from the system. For $X = O$ at the germinal center border this reaction mimics emigrating output cells. For $X = A$ it describes the loss of active antigen presenting sites due to the uptake of antigen portions by centrocytes.

B. Centroblast hypermutation

About 3 days after the initiation of the germinal center, centroblasts start to undergo somatic hypermutations while proliferating according to Eq. (1). Mutations in the genes that code for the antibody variable region of centroblasts may either increase, decrease or leave their affinity to antigen unchanged. In principle, centroblast hypermutation could be described within the well-known shape space concept [21], where each site of a high-dimensional lattice represents a particular antibody phenotype and a jump from one site to a neighboring site represents a mutation. In order to keep the model as simple as possible, we will apply a one-dimensional realization of this concept in terms of a number of affinity classes.

We assign to each centroblast a random variable n_a, which denotes its affinity class. The initial (germline) affinity class corresponds to $n_a = 0$ and we consider a total number of N_a affinity classes:

$$-N_d \leqslant n_a \leqslant N_d \text{ with } N_d \equiv \frac{N_a - 1}{2}. \tag{9}$$

Here, we defined the maximal mutation distance N_d and in what follows we will assume N_a to be an odd number. The progeny of a centroblast may change its affinity class with respect to its parents affinity class by $+1(-1)$ with probability $p_+(p_-)$ or preserve it it with probability $p_0 = 1 - p_+ - p_-$. This holds independent of the affinity class number, except for the highest and lowest affinity class numbers where we set, respectively, $p_+ = 0$ and $p_- = 0$.

In the process of centroblast differentiation according to Eq. (2) the affinity class is passed on to centrocytes that express the surface antibodies with corresponding affinity to antigen. We assume that centrocyte antibodies in two consecutive affinity classes differ in their binding reaction rate to antigen on follicular dendritic cells by a constant factor $\alpha > 1$:

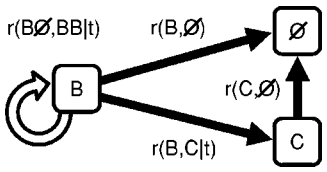

FIG. 2. Schematic representation of centroblast proliferation, apoptosis, and differentiation. See the text for details.

$$r_{n_a}(CA, C^\star A) = r_0(CA, C^\star A)\alpha^{n_a}. \tag{10}$$

It follows that centrocytes of different affinity classes surrounding the same antigen presenting site will compete for receiving the survival signal. The centrocyte with highest affinity and thus highest reaction rate will be most likely to reach this goal first. This affinity-based selection of centrocytes is expected to yield a strong population of high-affinity mutants.

Finally, we specify

$$\alpha \equiv \beta^{1/N_d}, \tag{11}$$

where $\beta > 1$ is referred to as the maximal affinity factor, so that

$$\frac{1}{\beta} \leqslant \frac{r_{n_a}(CA, C^\star A)}{r_0(CA, C^\star A)} \leqslant \beta, \tag{12}$$

independent of the maximal mutation distance N_d. This allows us to study affinity maturation in germinal center reactions as a function of the number of mutations required to achieve maximal antibody-antigen affinities.

C. Centroblast reaction regulation

Several days after the initiation of the reaction, a germinal center starts to develop into a compartmentalized microenvironment consisting of a dark and a light zone. The remarkable morphology of germinal centers must be related to the regulation of centroblast reaction processes. These are depicted in Fig. 2. In the framework of a stochastic and discrete model for germinal center morphology, it has been suggested that follicular dendritic cells may secrete signal molecules that diffuse through the system and initiate differentiation processes when consumed by centroblasts [11]. However, it is not known today whether such a differentiation signal does at all exist. A similar model takes chemotaxis into account, where the motion of diffusing cells follows a preferred direction that is specified by chemotactic signals [12,22]. However, the occurrence of a dark and a light zone in human germinal centers could not be explained by chemotaxis alone.

The mechanism for centroblast reaction regulation that gives rise to the specific spatial separation of centroblast and centrocyte is still unknown today. Therefore, in order to keep the model generic and simple, we opt for a phenomenological approach. From the experimentally observed germinal center morphology and related experiments we draw the conclusion that centroblast proliferation seems to be inhibited in the presence of follicular dendritic cells and T cells, while at the same time these environmental conditions seem to support the differentiation of centroblast into centrocyte [2,23–25]. Centroblasts undergo proliferation, apoptosis, and differentiation processes everywhere in the germinal center, while the centroblast population is diminished by the latter two processes and is increased by proliferation (see Fig. 2). After the first 3 days in which centroblasts have filled the whole germinal center, the light zone appears where follicular dendritic cells are located and T cells are present. The region that remains filled with centroblast becomes the dark zone and is disappearing with a delay of several days.

Environmental conditions that give rise to such a behavior are captured in the model in an effective way. We consider the centroblast proliferation rate $r(B\varnothing, BB|t)$ and the differentiation rate $r(B, C|t)$ to be time dependent, where differentiation is increasing on the cost of proliferation:

$$\frac{r(B,C|t)}{r(B,C)} = 1 - \frac{r(B\varnothing, BB|t)}{r(B\varnothing, BB)}. \tag{13}$$

Since environmental conditions are different in the light and dark zones, Eq. (13) is considered for both zones separately and is fulfilled by

$$r(B\varnothing, BB|t) = r(B\varnothing, BB) \times \{\Theta(y_b - y)F_d(t) + \Theta(y - y_b)F_l(t)\} \tag{14}$$

and

$$r(B,C|t) = r(B,C) \times \{\Theta(y_b - y)[1 - F_d(t)] + \Theta(y - y_b)[1 - F_l(t)]\}. \tag{15}$$

Here, $\Theta(s)$ is the step function with

$$\Theta(s) = \begin{cases} 1 & \text{for } s \geqslant 0, \\ 0 & \text{for } s < 0, \end{cases} \tag{16}$$

and y_b denotes the border between the dark and light zones, which, in accordance with the coordinate system shown in Fig. 1, extends along the x direction. The functions $F_d(t)$ and $F_l(t)$ refer to, respectively, the dark and light zones with $0 < F_i(t) \leqslant 1$ $(i = d, l)$. They are free to be chosen in such a way that the phenomenological approach represented by Eqs. (13)–(15) reproduces the germinal center morphology. It should be noted that this freedom is no unneeded luxury but is actually required to account for the fact that the experimentally observed appearance time and duration time of the compartmentalized structure can be quite different [2,23,26,27]. A useful representation with a high degree of flexibility is given by

$$F_i(t) = 1 + (f_i - 1)\frac{g(t, w_i, t_i)}{g(T_s, w_i, t_i)}, \tag{17}$$

where T_s denotes the simulation time and

$$g(t, w_i, t_i) = \tanh(w_i t_i) + \tanh[w_i(t - t_i)]. \tag{18}$$

The function $F_i(t)$ is decreasing with time over a time interval $2w_i^{-1}$ around $t = t_i$ from its initial value $F_i(0) = 1$ to its final value $F_i(T_s) = f_i$ with $0 < f_i \leqslant 1$. In total there is a set of three

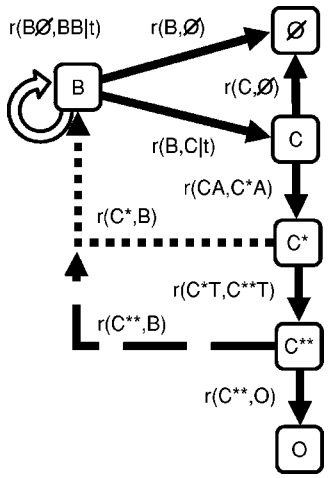

FIG. 3. Schematic representation of centrocyte-centroblast recycling. Two recycling pathways are depicted by a dotted and a dashed arrow. See the text for details.

parameters, $\{f_i;w_i;t_i\}$, to be specified per compartment $(i=d,l)$.

We finally address another issue that is related to making centroblast reaction regulation more realistic. The condition that centroblast proliferation is only possible if one of the nearest-neighbor sites is empty is relaxed by requiring that one out of the N_c closest neighbor sites has to be empty. The newly generated centroblast will then be located at the closest empty site.

D. Centrocyte-centroblast recycling

It has been suggested that not all positively selected centrocytes differentiate into output cells but may undergo recycling into centroblasts and reenter the process of proliferation, mutation and differentiation [3,28]. The advantage of such a recycling process is obvious. Positively selected centrocytes encode surface antibodies with high affinity for antigen and thus represent an optimal starting point for the reproduction of further optimized centroblasts. It should be noted, however, that there is no direct experimental proof that recycling is actually realized in germinal centers. As a consequence, no experimental values for parameters connected with the recycling hypothesis are available today.

In the present model we will assume that recycling is not restricted to one of the compartments but can occur anywhere throughout the germinal center. Two possible recycling pathways that differ in their starting point are depicted in Fig. 3. The dashed arrow refers to the recycling process that is commonly considered [3,4,7],

$$C^{\star\star} \rightarrow B \text{ with rate } r(C^{\star\star},B), \tag{19}$$

involving only centrocytes that have been positively selected by antigens and by T cells. The dotted arrow in Fig. 3 indicates another possibility involving $C^{\star}$ centrocytes,

$$C^{\star} \rightarrow B \text{ with rate } r(C^{\star},B). \tag{20}$$

These centrocytes only received the first survival signal from binding to antigen; however, with respect to their affinity they are equally well suited for recycling than $C^{\star\star}$ centrocytes. Because $C^{\star}$ centrocytes will be much earlier available in the course of the germinal center reaction than $C^{\star\star}$ centrocytes, it can be expected that the effect of the two recycling pathways on the system's time evolution will be quite different. The combination of the two recycling pathways,

$$C^{\star,\star\star} \rightarrow B \text{ with rate } r(C^{\star,\star\star},B), \tag{21}$$

is a third possible realization of recycling in germinal centers that will be considered within our model.

It should be noted that centrocyte-centroblast recycling may be also of a disadvantage with respect to the total number of output cells. Once the centrocyte changes into a centroblast, it is again subjected to apoptosis and will be lost if it does not sufficiently soon differentiate into a centrocyte and receive the first survival signal again.

IV. STOCHASTIC DISCRETE EVENT ALGORITHMS

In the previous section, we introduced a reaction-diffusion model that describes a germinal center reaction on a d-dimensional lattice with N sites. Each site can either be occupied by one type of cell or be empty. The actual configuration on the lattice defines the system state and determines whether a particular reaction process is enabled—i.e., can take place—or not. Each reaction process changes the lattice configuration into another configuration that usually differs from the previous one only in a small region around the reaction sites.

The change of the system state is related to the time that elapses between the moment that a particular reaction process becomes enabled and the moment that it actually takes place. For one and the same reaction type this amount of time varies and depends on several factors—e.g., the energy and the condition of the involved cells—which are not explicitly part of the model. However, we incorporate these factors on the reaction times by describing the occurrence of reactions in a stochastic manner. To this end we have to formulate a fundamental assumption that defines the kinetics for non-negative reaction rates which may change continuously as a function of time. Following Refs. [15,16], where the kinetics assumption has been stated for constant reaction rates, we assume that *the reaction process with rate* $r(c,c'|t)$ *that changes the system state* c *into* c' *and that is enabled at time* t *occurs with probability*

$$p(c,c'|t,t+\delta t) = r(c,c'|t)\delta t \tag{22}$$

in the infinitesimal time interval δt. In other words, the probability that an enabled reaction occurs is equal to its reaction rate times an infinitesimal time interval δt, which is sufficiently small to neglect the probability for two reactions occurring simultaneously.

It follows directly from Eq. (22) that the system state c at time t is now a stochastic variable which is realized with some probability $P(c|t)$. We show that the time evolution of this probability distribution is governed by a master equation. The probability $P(c|t+\delta t)$ to find the system in configuration c at time $t+\delta t$ is given by

$$P(c|t+\delta t) = P(c'|t) \sum_{c' \neq c} p(c',c|t,t+\delta t) + P(c|t)p(c,c|t,t+\delta t). \quad (23)$$

Here, the first term accounts for changes of the system state $c'(\neq c)$ at time t into system state c at time $t+\delta t$. The second term accounts for the possibility that the system, which is already in system state c at time t, remains in this state with probability

$$p(c,c|t,t+\delta t) = 1 - \delta t \sum_{c' \neq c} r(c,c'|t). \quad (24)$$

We may thus write

$$P(c|t+\delta t) = P(c|t) - \delta t \sum_{c' \neq c} [P(c|t)r(c,c'|t) - P(c'|t)r(c',c|t)], \quad (25)$$

which yields, in the limit $\delta t \to 0$,

$$\frac{d}{dt}P(c|t) = \sum_{c' \neq c} [P(c'|t)r(c',c|t) - P(c|t)r(c,c'|t)], \quad (26)$$

and corresponds to the master equation for the probability distribution $P(c|t)$.

In the present context we are not merely interested in studying a system at equilibrium, where Eq. (26) simplifies because $dP(c|t)/dt=0$. We rather wish to simulate the full time evolution of a germinal center reaction, which amounts to solving the master equation (26) for all times.

In practice we will not compute the probability $P(c|t)$ explicitly, but start from a particular system state, representative for the initial state of the germinal center, and then generate in the course of time a sequence of system states with the correct probability. This requires the calculation of the time at which the next reaction occurs and is achieved as follows: Supposing that the system is in state c at time t, we calculate the probability that the system remains in this state until time $t+\tau$. The master equation (26) reduces to

$$\frac{d}{dt}P(c|t) = -P(c|t) \sum_{c' \neq c} r(c,c'|t). \quad (27)$$

Integration between the limits t and $t+\tau$ yields

$$P(c|t+\tau) = \exp\left[- \sum_{c' \neq c} \int_0^\tau d\tilde{t}\, r(c,c'|t+\tilde{t}) \right], \quad (28)$$

where we used the fact that the system is in state c at time t: $P(c|t)=1$. A simplification of this expression is possible if the dependence of the reaction rates on time is negligibly weak on the time scale where no reaction takes place. The integral in Eq. (28) may then be approximated by

$$\int_0^\tau d\tilde{t} r(c,c'|t+\tilde{t}) = r(c,c'|t)\tau + \frac{1}{2} \left. \frac{dr(c,c'|t+\tilde{t})}{d\tilde{t}} \right|_{\tilde{t}=0} \times \tau^2 + \mathcal{O}(\tau^3). \quad (29)$$

In fact, in the context of the reaction-diffusion model for germinal centers it turns out that the second term on the right-hand side in Eq. (29) is always orders of magnitude smaller than the first term (see Sec. V A below). It can therefore be neglected which corresponds to applying the adiabatic approximation,

$$r(c,c'|t) \approx r(c,c'|t+\tau), \quad (30)$$

on the time scale where no reaction takes place. We then obtain a negative exponential distribution function for the probability that no reaction occurs between t and $t+\tau$,

$$P(c|t+\tau) = \exp[-\tau R(c|t)], \quad (31)$$

where we defined

$$R(c|t) \equiv \sum_{c' \neq c} r(c,c'|t). \quad (32)$$

Next, we calculate the probability for the occurrence of the particular reaction $c \to \tilde{c}$. The probability that this reaction occurs in the infinitesimal time interval $\delta\tau$ follows from Eqs. (22) and (30) to be

$$p(c,\tilde{c}|t+\tau,t+\tau+\delta\tau) = r(c,\tilde{c}|t)\,\delta\tau. \quad (33)$$

We combine Eqs. (31) and (33) to obtain the probability that the system, which was in state c at time t, is in state $\tilde{c}$ at time $\tilde{t} \equiv t+\tau+\delta\tau$:

$$P(\tilde{c}|\tilde{t}) = P_{\tilde{c}} P_\tau. \quad (34)$$

Here, we defined the probability distribution for reactions,

$$P_{\tilde{c}} \equiv \frac{r(c,\tilde{c}|t)}{R(c|t)}, \quad (35)$$

which is independent of the probability distribution for waiting times,

$$P_\tau \equiv [\delta\tau R(c|t)]\exp[-\tau R(c|t)], \quad (36)$$

corresponding to a negative exponential distribution.

We conclude from the above that an algorithm for the stochastic discrete event simulation of a reaction-diffusion system is based on the following two choices per time step: (i) the type of enabled reaction according to the distribution $P_{\tilde{c}}$ and (ii) the waiting time τ according to the distribution P_τ. This approach has been introduced by Gillespie in the context of chemical reactions in solutions and is referred to as the direct method [15]. We implemented a slightly different method, also invented by Gillespie, which is called the first reaction method and was proven to be mathematically equivalent to the direct method [16]. We also implemented a modification of the first reaction method, which increases the efficiency of that algorithm by making use of the fact that each reaction changes the lattice configuration only in a small region around the reaction sites. It was developed by Gibson and Bruck and is referred to as the next reaction method [17]. We will briefly discuss these and other methods in the context of germinal center reactions in the following subsections.

A. First reaction method

The type of an enabled reaction and the waiting time do not necessarily have to be generated in a direct way from the distributions Eqs. (35) and (36), as is the case in the direct method. Alternatively, one can also determine a putative waiting time for each enabled reaction at each site of the lattice in a particular system state. For a reaction process that changes the system state c at time t into c', the corresponding waiting time τ' follows from Eq. (36) to be given by

$$\tau' = \frac{1}{r(c,c'|t)} \ln\left(\frac{1}{u}\right), \tag{37}$$

where u is a random number that is generated from the uniform distribution with $0 < u \leqslant 1$. Then, of all the enabled reactions, the reaction to be performed is the one which comes first—i.e., the one with the shortest waiting time.

The algorithm of the first reaction method reads [16] as follows:

(i) *initialize the system at* $t=0$ *and set the total simulation time* T_s

(ii) *at each site of the lattice generate for each enabled reaction a putative waiting time according to Eq. (37)*

(iii) *choose the reaction process with the shortest waiting time,* τ_s*, and execute the reaction process*

(iv) *set* $t \leftarrow t+\tau_s$

(v) *repeat all steps from step (ii) until* $t=T_s$

This algorithm requires computation time proportional to the number of reactions in the system state, N_r, which is proportional to the number of lattice sites times the number of reaction processes. Furthermore, N_r random numbers have to be newly generated per iteration.

B. Next reaction method

The number of newly generated random numbers and the computation time are significantly decreased in the next reaction method with respect to the first reaction method. This is achieved by realizing that reusing generated waiting times is admitted [17]. Because a reaction process changes the system state only locally, putative waiting times have to be generated per iteration for each enabled reaction at a few sites only.

We implemented the algorithm of the next reaction method in the following way:

(i) *initialize the system at* $t=0$ *and set the total simulation time* T_s

(ii) *at each site of the lattice generate for each enabled reaction a putative waiting time according to Eq. (37)*

(iii) *choose the reaction process with the shortest waiting time,* τ_s*, and execute the reaction process*

(iv) *set* $t \leftarrow \tau_s$

(v) *at each reaction site of the lattice generate for each enabled reaction a putative waiting time according to Eq. (37)*

(vi) *repeat all steps from step (iii) until* $t=T_s$

It is obvious that this algorithm requires much fewer operations and must be faster than the one of the first reaction method, because step (v) involves only the one or two reaction sites instead of all lattice sites. The precise gain in computation time depends strongly on the implementation of appropriate data structures [17]. In view of the limited abilities of random number generators, we also mention the advantage that only a few random numbers have to be generated per iteration. The precise number depends on the previous reaction process and on the considered lattice configuration, but will usually be less than two times the number of nearest neighbor sites. Finally, it should be noticed from step (iv) that in the next reaction method the waiting times are absolute times and not relative times between reaction processes.

C. Other simulation methods

The two simulation methods described in the previous subsections belong to a class of algorithms that is derived from the dynamical Monte Carlo technique [18,29,30]. In contrast to the classical Monte Carlo technique, which is employed to study systems at equilibrium, the dynamical Monte Carlo technique provides methods to solve the time evolution of a system. The different methods have their own right of existence since they have been invented to optimize the use of computer resources—i.e., computer time and memory—for specific types of problems.

We briefly mention another method of the dynamical Monte Carlo technique, which is called the random selection method and has become quite popular in recent years. The algorithm in its most simple form consists essentially of choosing per time step (i) a location on the lattice with probability $1/N$ and (ii) a type of reaction process [18]. The latter is chosen with probability r_p/R_P, where $R_P=\Sigma_{p=1}^{P} r_p$ and r_p denotes the rate of the pth out of P possible reaction processes. All reaction processes are assumed to be constant in time and thus independent of the actual system state. Then, if possible, the randomly chosen reaction process is carried out at the randomly chosen location on the lattice and the procedure is repeated. This method is very efficient, provided that reaction processes are accepted often, and has also been applied to simulate germinal center reactions [11,12,22]. It should be noted, however, that the random selection method can only be applied if the reaction rates do not depend on time, because this method decouples the notion of time from the simulation. It essentially corresponds to a discretization of the master equation (26) with a fixed time step $1/(NR_P)$, independent of the system state and the reaction process to be performed. Therefore, the random selection method should only be applied to reaction-diffusion systems with time-independent reaction rates and if the main goal is not simulating the system's exact time evolution.

A different approach for simulating reaction-diffusion systems is known as the cellular automata technique [31]. The dynamics of a cellular automaton, where each site of the lattice corresponds to a computational cell, is characterized by a simultaneous update of all these cells in each iteration step according to predefined deterministic rules. In contrast to the methods of the dynamical Monte Carlo technique, which are inherently serial in time, cellular automata modeling allows for efficient implementations on massive parallel computers. However, the notion of time is lost completely in this case because slow and fast reactions have the same prob-

ability to occur in a simultaneous cell update. The dynamics of a stochastic system cannot be correctly simulated in this way. As a way out, cellular automata modeling with nondeterministic rules have been proposed, where a certain reaction process occurs with a probability that depends again on the rate constants. If this is done in such a way that the master equation (26) is satisfied, then the algorithm for the nondeterministic cellular automaton resembles that of the random selection method [29].

We conclude that the first reaction method and the next reaction method are exact and general methods for the stochastic discrete event simulation of reaction-diffusion systems with respect to the system's time evolution. In comparison with other simulation methods these algorithms demand relatively large computer resources; however, this does not pose a serious problem in the present context of germinal centers because of the moderate system size.

V. NUMERICAL SIMULATIONS

In this section, we present the results obtained from stochastic discrete event simulations of germinal center reactions using both the first reaction method and the next reaction method. We first summarize the model parameters and initial conditions and then compare the first reaction method and the next reaction method with each other. Next, we present the simulation results for particular germinal center properties, such as their morphology, affinity maturation, and recycling.

A. Model parameters and initial conditions

The germinal center is represented by the reaction-diffusion model on a two-dimensional square lattice of equidistant sites with lattice constant a. The lattice has a circular geometry with a diameter of 130 sites. The total number of $N=13273$ lattice sites provides sufficient space for the occurrence of realistic cell populations. The antigen presenting sites are kept fixed throughout the simulation at random positions in the upper 70% of the system volume. In this way we mimic the accommodation of antigen presenting sites by follicular dendritic cells without actually representing the latter. As a consequence all cells can diffuse freely without being hindered by the presence of the follicular dendritic cells. It might be argued that this makes the two-dimensional simulation system actually more comparable to the three-dimensional germinal center, where the presence of follicular dendritic cells do hinder free cell diffusion.

In Table I we summarize the model parameters and initial conditions that we use in the simulations, if not stated otherwise. The reaction rates are measured in units of inverse days (d^{-1}). We note that the choice of these parameters as obtained from the literature is to be understood as a starting point in the high-dimensional parameter space. In general it is actually not clear *a priori* how microscopic rate constants of the stochastic discrete event simulation are related to experimentally determined average reaction times. For example, an important aspect that is completely missing in a macroscopic view on biological systems is the availability of free space. The limitation of empty sites gives rise to a competition between increasing cell populations and strongly influences the mixing of different cell types that first have to meet in order to undergo a reaction process.

TABLE I. Model parameters and initial conditions.

Parameter	Value	Remark
$r(B\varnothing, BB)$	4 d^{-1}	[2,12,26]
N_c	8 sites	
$r(B,C)$	4 d^{-1}	[11,22]
$\{f_d; w_d; t_d\}$	$\{0.2; 0.4\ d^{-1}; 10\ d\}$	
$\{f_l; w_l; t_l\}$	$\{0.2; 0.4\ d^{-1}; 6\ d\}$	
$r_0(CA, C^\star A)$	0.2 d^{-1}	[13,32,33]
$\{N_a; \beta; p_+; p_-\}$	{7; 100; 0.33; 0.33}	[4]
$r(\varnothing, T)$	0.02 d^{-1}	
$r(C^\star T, C^{\star\star} T)$	4 d^{-1}	
$r(C^{\star\star}, O)$	4 d^{-1}	[11,22]
$r(B\varnothing, \varnothing B)$	1.25 d^{-1}	$R_B \approx 7.5\ \mu$m
$r(X\varnothing, \varnothing X)$	3.75 d^{-1}	$R_X \approx 2.5\ \mu$m
$X = C, C^\star, C^{\star\star}$		
$r(T\varnothing, \varnothing T)$	2 d^{-1}	$R_T \approx 5\ \mu$m
$r(O\varnothing, \varnothing O)$	2 d^{-1}	$R_O \approx 5\ \mu$m
$r(T, \varnothing)$	0.8 d^{-1}	[34]
$r(B, \varnothing)$	0.8 d^{-1}	[35]
$r(C, \varnothing)$	4 d^{-1}	[36]
$r(A, \varnothing)$	0.03 d^{-1}	[37]
$A(t=0)$	400	[38–40]
$B(t=0)$	5	[26,41,42]
T_s	21 d	[2]

Jump processes of cells from site to site on the lattice are modeled by relating the reaction rates to the corresponding diffusion constants. The latter are estimated following the approach in Ref. [11], where the diffusion constant D_X is assumed to obey the well-known Stokes-Einstein relation $D_X = k_B T_0 / (6\pi\eta_b R_X)$. Here, k_B is the Boltzmann constant, T_0 is the room temperature, $\eta_b = 0.02\ \mathrm{J\,s\,m^{-3}}$ is the blood viscosity [43], and R_X is the radius of the corresponding cell type X (see Table I). The model takes different cell sizes effectively into account by relating the lattice constant to the arithmetic mean cell radius: $a = 2(R_B + R_C + R_T + R_O)/4 = 10\ \mu$m. The reaction rates for site-to-site jump processes on the square lattice are obtained from the diffusion constants by $r(X\varnothing, \varnothing X) = D_X / a^2$ and the corresponding values are given in Table I.

The centroblast reaction regulation in the light and dark zones is modeled by proliferation and differentiation rates that depend on time. In Fig. 4 we plot the time-dependent part of the proliferation rates according to Eq. (17) and for the parameters given in Table I. The time is measured in units of days (d). The only difference between $F_d(t)$ and $F_l(t)$ lies in the choice of t_d and t_l, respectively, from which we expect the following scenario. In the light zone centroblast

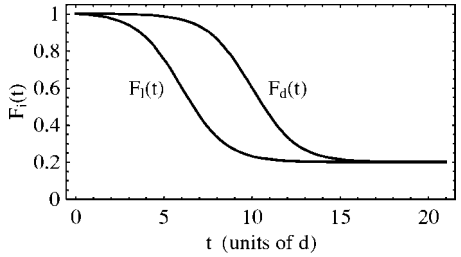

FIG. 4. The functions $F_d(t)$ and $F_l(t)$ according to Eq. (17) for the parameters given in Table I.

differentiation should start to dominate over proliferation around $t_l - w_l^{-1} = 3.5$ d, while the dark zone should start to disappear around $t_d - w_d^{-1} = 8.5$ d and should be vanished around $t_d + w_d^{-1} = 12.5$ d.

Finally, we consider the validity of the adiabatic approximation that we applied in going from Eq. (28) to Eq. (31). The slope of $F_i(t)$ is maximal at $t = t_i$ and we estimate that

$$\left| \frac{1}{2} \frac{dF_i(t)}{dt} \right| \leqslant \frac{w_i |f_i - 1|}{2g(T, w_i, t_i)} \sim \mathcal{O}(10^{-2}) \mathrm{d}^{-1}. \tag{38}$$

Furthermore, $F_i(t_i) \sim \mathcal{O}(10^{-1})$ and in the simulations the typical waiting time is of the order $\tau \sim \mathcal{O}(10^{-5})$ d. It follows that the main contribution in the expansion Eq. (29) stems indeed from the first term, since

$$1 \gg \frac{\tau}{F_i(t_i)} \left| \frac{1}{2} \left. \frac{dF_i(t)}{dt} \right|_{t=t_i} \right| \sim \mathcal{O}(10^{-6}). \tag{39}$$

We conclude that applying the adiabatic approximation, Eq. (30), with the benefit of significant computational simplifications is fully justified.

B. Comparison of simulation methods

We discuss the results of a systematic comparison of germinal center reactions simulated by the first reaction method and the next reaction method. To this end we performed 20 simulations per simulation method using the model parameters and initial conditions given by Table I for different random initial configurations. It is obvious that, independent of the applied simulation method, small changes in the initial phase of the reaction can give rise to recognizable differences in the progression of the reaction. For example, if one or two of the initially present B cells happen to undergo apoptosis before they could start to proliferate, then the filling of the germinal center by centroblasts will be retarded affecting its further development.

A quantitative comparison of the first reaction method and the next reaction method in terms of the number of antigen presenting sites and cells as a function of time is presented in Fig. 5. The width of the curves corresponds to two times the sample standard deviation taken over the 20 simulations. In Table II we present the corresponding values of the final numbers for antigen presenting sites and cells.

This comparison shows that the first reaction and next reaction methods produce results that are, as expected, in excellent quantitative agreement. Computing a germinal center reaction using the next reaction method is, however, by a factor 6–8 faster. Therefore, in what follows we use the next reaction method to study properties of germinal centers.

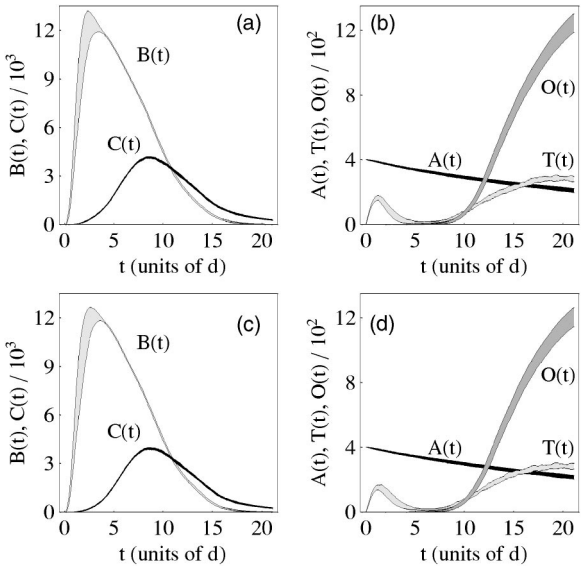

FIG. 5. The number of antigen presenting sites and cells as a function of time for 20 simulations using the first reaction method [(a) and (b)] and the next reaction method [(c) and (d)]. The width of the curves corresponds to two times the sample standard deviation.

C. Morphology of germinal centers

The development of the germinal center morphology in the course of time is depicted in Fig. 6 as obtained from a typical stochastic discrete event simulation. For reasons of clarity only antigen presenting sites (black), centroblasts (light gray), and centrocytes (dark gray) are shown and their numbers are given in Table III together with those of the T cells and the output cells.

The initial configuration consists of 400 antigen presenting sites in the upper part of the system and five randomly positioned B cells [see Fig. 6(a)]. The centroblasts proliferate and start to fill the whole germinal center [see Fig. 6(b)] until it is completely filled at day 3 [see Fig. 6(c)]. Thus, nearly all antigen presenting sites are now surrounded by centroblasts, which start to undergo hypermutation and differentiation into

TABLE II. Quantitative comparison of the final number of antigen presenting sites and cells in terms of the mean value and the sample standard deviation for the simulations of Fig. 5.

Number at $t = 21$ d	First reaction method	Next reaction method
A	210 ± 12	214 ± 11
T	281 ± 15	284 ± 16
B	5 ± 5	9 ± 9
C	267 ± 23	255 ± 25
O	1244 ± 51	1205 ± 59

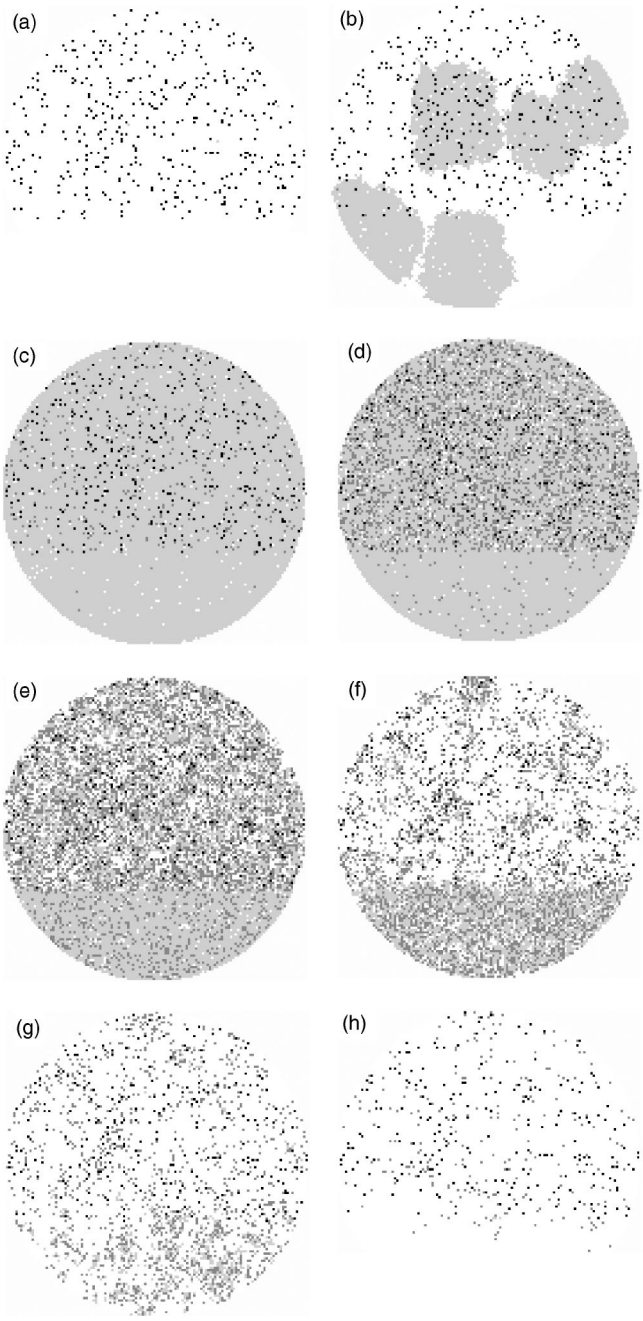

FIG. 6. Development of the germinal center morphology in the course of time. Snapshots are taken at (a) day 0, (b) day 1, (c) day 3, (d) day 6, (e) day 9, (f) day 12, (g) day 15, and (h) day 21. For reasons of clarity only antigen presenting sites (black), centroblasts (light gray), and centrocytes (dark gray) are shown. The corresponding numbers are given in Table III.

centrocytes. Based on the affinity of their surface receptors to antigen the centrocytes around the antigen presenting cells will compete for the first survival signal. As a consequence of the relatively high death rate of nonselected centrocytes, the populous germinal center starts to thin out where centroblast differentiation is strongest, which is the case in the vicinity of the follicular dendritic cells. The germinal center develops into a compartmentalized microenvironment with a light and a dark zone that are clearly distinguishable at day 6 [see Fig. 6(d)]. With a delay of a few days, the dark zone starts to disappear [see Fig. 6(e)] and is practically vanished at day 12 [see Fig. 6(f)] where it contains roughly as many centrocytes as centroblasts.

TABLE III. The number of antigen presenting sites and cells as a function of time corresponding to the snapshots of the germinal center reaction depicted in Fig. 6.

Fig. 6	t (d)	A	T	B	C	O
(a)	0	400	0	5	0	0
(b)	1	388	132	5402	14	0
(c)	3	368	49	12257	388	0
(d)	6	335	20	9705	2621	1
(e)	9	307	50	5792	3955	24
(f)	12	287	162	2234	2700	287
(g)	15	269	235	556	1316	693
(h)	21	223	281	3	233	1223

In the meantime the T cell population in the light zone increases again due to the availability of space (see Table III). The light zone becomes a dilute system of interacting cells [see Figs. 6(f) and 6(g)], which is actually required to enhance the probability that positively selected centrocytes meet T cells and receive the second survival signal. In other words, as important as the initial dense filling of the germinal center by centroblasts is in order to obtain centrocytes close to the fixed antigen presenting sites, it is important that the germinal center evolves into a dilute cell system in order to increase the probability for the encounter of diffusing centrocytes and T cells. According to Table III this development of the germinal center morphology is indeed accompanied by an increase in the number of output cells. At the end of the germinal center reaction [see Fig. 6(h)], the number of antigen presenting cells is decreased by about 50% and also the number of centroblasts and centrocytes is again significantly decreased.

We thus see that our reaction-diffusion model captures the experimentally observed development of the germinal center morphology very well.

D. Antibody-antigen affinity maturation

Hypermutation of centroblasts and selection of centrocytes are the main pillars of affinity maturation aiming to yield a strong population of mutants with high antibody-antigen affinity. As has been explained in Sec. III B, we model the hypermutation of centroblasts within the simple picture of affinity classes and the selection of centrocytes based on their affinity to antigen. We study affinity maturation as a function of the maximal mutation distance N_d. This number corresponds to the mutation steps required for a centroblast to go directly from the germline affinity class with reaction rate $r_0(CA, C^*A)$ to the highest affinity class with reaction rate $r_{N_d}(CA, C^*A) = \beta r_0(CA, C^*A)$. We note that the germline affinity, which is directly related to $r_0(CA, C^*A)$, is the same in all simulations.

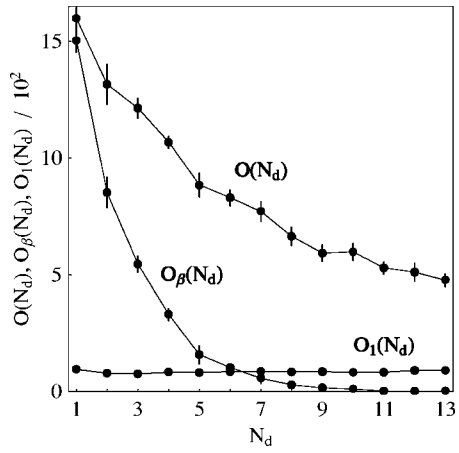

FIG. 7. The number of output cells (dots) as a function of the maximal mutation distance N_d. This plot is the result of 65 simulations using the parameter values and initial conditions as given in Table I for different random initial conditions. The size of the error bars corresponds to two times the sample standard deviation and the solid lines are a guide to the eye.

We performed 65 simulations using the parameter values and initial conditions as given in Table I for different random initial conditions. In Fig. 7 we plot the number of output cells as a function of N_d. We denote the total number of output cells by $O(N_d)$, while the numbers of output cells belonging to the germline affinity class and the highest affinity class are denoted by, respectively, $O_1(N_d)$ and $O_\beta(N_d)$. We observe that $O(N_d)$ is an exponentially decreasing function of N_d that levels off for large values $N_d \gg 10$. At $N_d = 50$ we find that $O(N_d)$ is still of the order of 300 output cells (result not shown). Furthermore, we notice that $O_1(N_d)$ is practically independent of N_d, whereas $O_\beta(N_d)$ is strongly affected and exponentially diminished to zero around $N_d = 13$. This means that the decrease in the total number of output cells is mainly paid for by the high-affinity output cells.

In Fig. 8 we plot the relative numbers of output cells $\Omega_\beta(N_d) = O_\beta(N_d)/O(N_d)$ and $\Omega_1(N_d) = O_1(N_d)/O(N_d)$. It is clearly seen that the result of a germinal center reaction depends strongly on the maximal mutation distance with a crossover at $N_d = 6-7$. At small maximal mutation distances $N_d < 5$, most output cells belong to high-affinity classes and in the limit $N_d = 1$ nearly all of them are of the highest-affinity class. The opposite is true for large maximal mutation distances $N_d > 9$, where the affinity of most of the output cells does not really improve during the germinal center reaction but remains low and distributed over affinity classes close to that of the germline. Therefore, we conclude that the maximal mutation distance between the germline affinity and the optimal affinity is of great importance for the success of a germinal center reaction with respect to the affinity maturation.

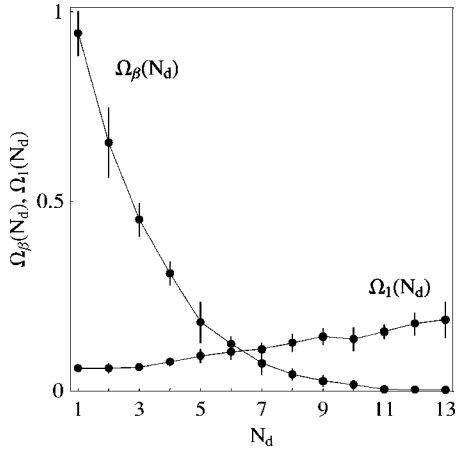

FIG. 8. The relative number of output cells, $\Omega_\beta(N_d) = O_\beta(N_d)/O(N_d)$ and $\Omega_1(N_d) = O_1(N_d)/O(N_d)$, as obtained from the data in Fig. 7. The solid lines are a guide to the eye.

Our numerical results are in agreement with experimental evidence that the upper limit for relevant maximal mutation distances is around $N_d = 12$ [44,45]. Furthermore, our results provide an explanation for another experimental finding in germinal centers: namely, that they either contain no high-affinity output cells at all or are dominated by output cells of high affinity [46,47]. This global all-or-none behavior is the reflection of a local winner-takes-all mechanism. In the present model, the winner-takes-all mechanism is due to reaction rates that depend on the affinity and that induce a competition for the survival signal between centrocytes surrounding the same antigen presenting site. Within a hybrid cellular automata model for cell sorting, global all-or-none behavior has been observed due to a similar local winner-takes-all mechanism, where centrocyte selection takes place based on cellular adhesion which in turn is related to the affinity [13]. Affinity maturation has also been studied within a much more involved implementation of the shape space concept [48]. As far as a comparison is possible, our results agree surprisingly well with those obtained in the latter study.

E. Centrocyte-centroblast recycling

We study the impact of recycling on affinity maturation during germinal center reactions. For this purpose we performed 215 simulations using the parameter values and initial conditions as given in Table I for different random initial conditions. As has been discussed in Sec. III D, recycling may be realized by one of the three reaction processes, Eqs. (19)–(21), that are depicted in Fig. 3. In what follows, we will refer to the reaction process $C^{\star\star} \to B$ as type-I recycling, to $C^{\star} \to B$ as type-II recycling, and to $C^{\star,\star\star} \to B$ as type-III recycling.

In Fig. 9 we plot the number of output cells and the recycling probability as a function of the corresponding recycling rate, which we abbreviate by r_R. The recycling probability, p_R, is computed as the number of recycling events that have been performed during the germinal center reaction over the number of recycling events that could at most have been performed. It is obvious from Figs. 9(a) and 9(b) that, independent of the recycling type, the number of output cells is exponentially decreasing with increasing recycling rate. However, this decrease occurs significantly faster for type-II recycling as compared with type-I recycling. This is ex-

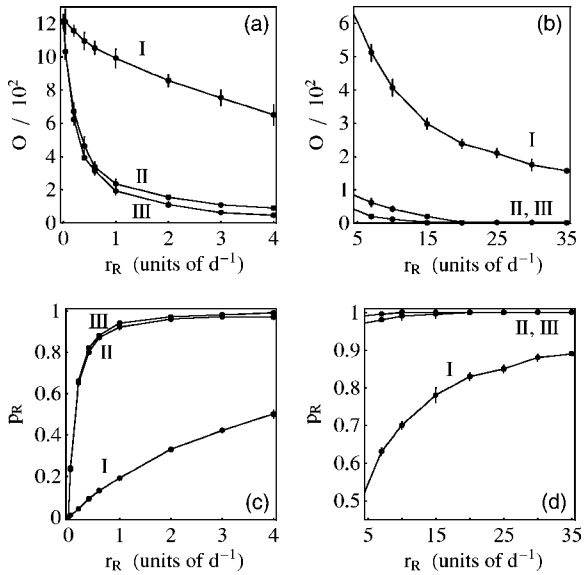

FIG. 9. The number of output cells [(a) and (b)] and the corresponding recycling probability [(c) and (d)] as a function of r_R for the three recycling types. This plot is the result of 215 simulations using the parameter values and initial conditions as given in Table I for different random initial conditions. The size of the error bars corresponds to two times the sample standard deviation and the solid lines are a guide to the eye.

plained by the fact that type-I recycling consumes $C^{\star\star}$ centrocytes, while type-II recycling consumes $C^{\star}$ centrocytes which are several days earlier available during the germinal center reaction. Thus, the time difference in the availability of $C^{\star}$ and $C^{\star\star}$ centrocytes plays an important role, which is reaffirmed by the fact that type-III recycling, consuming both $C^{\star\star}$ and $C^{\star}$ centrocytes, behaves very similar to type-II recycling. The recycling probability, which is plotted in Figs. 9(c) and 9(d), reflects this situation once again. At $r_R = 1\ \mathrm{d}^{-1}$ we find $p_R > 90\%$ for type-II and type-III recycling while still $p_R < 20\%$ for type-III recycling. Only for much higher recycling rates around $r_R = 35\ \mathrm{d}^{-1}$ do we obtain a type-I recycling probability of 90%.

Affinity maturation will only be improved by a recycling mechanism that operates in a parameter region where the recycling probability is large and the loss of output cells is small. In principle, this is the case for type-I recycling at recycling rates $7\ \mathrm{d}^{-1} < r_R < 30\ \mathrm{d}^{-1}$ and for type-II and type-III recycling at recycling rates $0.2\ \mathrm{d}^{-1} < r_R < 1\ \mathrm{d}^{-1}$. Since the number of output cells in type-III recycling is even smaller than that in type-II recycling, we will focus in what follows on the comparison of type-I and type-II recycling.

In Fig. 10 we plot the relative number of output cells with highest affinity, $\Omega_\beta = O_\beta / O$, and with germline affinity, $\Omega_1 = O_1 / O$, as a function of the recycling rate r_R for type-I and type-II recycling. We note that the size of the error bars increases with r_R due to the decrease in the number of output cells. It can be clearly seen that affinity maturation is improved by type-II recycling. The percentage of highest affinity mutants is increasing from about 45% at $r_R = 0\ \mathrm{d}^{-1}$ to about 68% at $r_R = 1\ \mathrm{d}^{-1}$, while in the same interval for r_R the relative number of output cells with germline affinity is decreasing from about 6% to 1%. Similar numbers are obtained for type-III recycling (results not shown). We do not observe any improvement of affinity maturation by type-I recycling, as was expected for this parameter region. However, we find that this is also not the case in the region of large recycling rates. In Fig. 11 we plot the relative number of output cells Ω_β and Ω_1 as a function of the recycling rate $r_R > 5\ \mathrm{d}^{-1}$ for type-I recycling. The percentage of highest-affinity mutants is approximately constant and lies around 50% and the relative number of output cells remains around 6%.

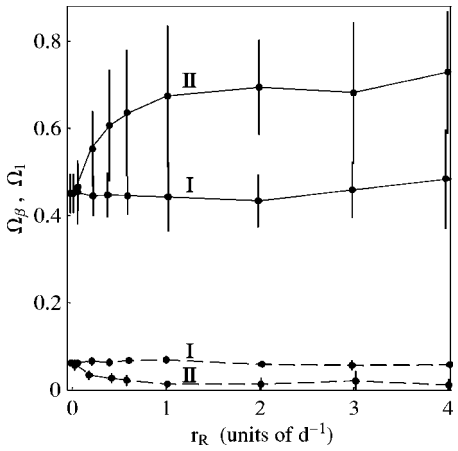

FIG. 10. The relative number of output cells $\Omega_\beta = O_\beta / O$ (solid lines) and $\Omega_1 = O_1 / O$ (dashed lines) as a function of the recycling rate r_R for type-I and type-II recycling. The solid and dashed lines are a guide to the eye.

Our model predicts that recycling of type I, which is based on $C^{\star\star}$ centrocytes, does not provide a significant improvement of affinity maturation but does give rise to an unwanted strong decrease in the number of output cells. This can be deduced from the absolute and relative numbers of output cells which are summarized in Table IV. For type-II recycling, which is based on $C^{\star}$ centrocytes, the decrease in the number of output cells is less severe and at the same time affinity maturation is optimized, resulting in a number of

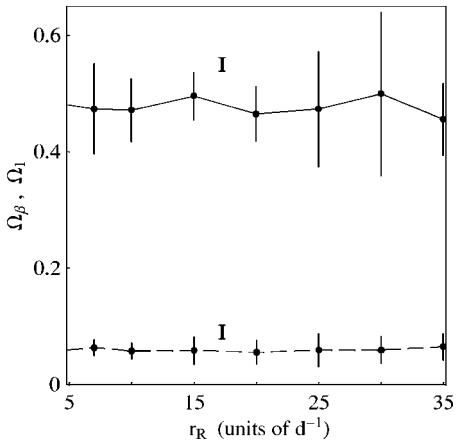

FIG. 11. The relative number of output cells, $\Omega_\beta = O_\beta / O$ (solid line) and $\Omega_1 = O_1 / O$ (dashed line), as a function of the recycling rate r_R for type-I recycling. The solid and dashed lines are a guide to the eye.

TABLE IV. Absolute and relative numbers of output cells for all three recycling types. These numbers are based on 50 simulations using the parameter values and initial conditions as given in Table I for different random initial conditions.

Recyc.	p_R	r_R (d^{-1})	O	O_β and Ω_β	O_1 and Ω_1
None	0	0	1213±43	545±33	75±2
				0.45±0.04	0.06±0.00
I	0.65	7	511±24	240±27	32±5
				0.47±0.08	0.06±0.01
II	0.65	0.2	671±50	367±29	22±4
				0.55±0.08	0.03±0.01
III	0.65	0.2	622±35	345±25	23±8
				0.56±0.07	0.04±0.01
I	0.80	15	298±16	147±4	17±6
				0.50±0.04	0.06±0.02
II	0.80	0.4	463±55	274±25	12±3
				0.61±0.13	0.03±0.01
III	0.80	0.4	392±12	226±12	10±2
				0.58±0.05	0.03±0.01
I	0.88	30	175±17	85±16	10±3
				0.50±0.14	0.06±0.02
II	0.88	0.6	335±33	208±27	7±3
				0.63±0.14	0.02±0.01
III	0.88	0.6	314±27	188±13	5±3
				0.60±0.09	0.02±0.01

high-affinity output cells that is larger than that for type-I recycling. Recycling of type III, which includes both $C^\star$ and $C^{\star\star}$ centrocytes, shows a behavior that is very similar to type-II recycling. It should be noted, however, that type-III recycling does not seem to improve type-II recycling. We may therefore conclude that the preferred recycling mechanism is of type II. However, for any type of recycling our simulations predict a significant decrease in the number of output cells, even in the subclass of high-affinity output cells. It therefore remains somewhat questionable whether recycling in germinal centers is an efficient mechanism at all.

To the best of our knowledge, recycling in germinal centers, where the interaction between $C^\star$ centrocytes and T cells is explicitly included in a microscopic model, has not been studied before. In previous microscopic models this part of the germinal center reaction has been neglected and an effective recycling mechanism was implemented that happens to resemble the type-II recycling mechanism [11,12,22,48].

VI. SUMMARY AND CONCLUSIONS

In this paper, we studied germinal center reactions by stochastic discrete event simulations within a microscopic reaction-diffusion model. We applied the philosophy that *everything should be made as simple as possible, but not simpler* [14] by introducing a generic model but applying exact simulation methods. To simulate the time evolution of complex and highly dynamic biological systems like germinal centers, it is indispensable necessary to perform stochastic discrete event simulations in an accurate way, because various coupled reaction processes occur on different characteristic time scales in a spatially compartmentalized microenvironment. In principle, the type of enabled reaction and the waiting time have to be chosen from the corresponding distributions at each time step. We have shown for the case of germinal center reactions that this is realized in an efficient way by the next reaction method [17] which we compared to the first reaction method [16].

Beside basic reaction processes—such as diffusion, birth, death, and survival processes—our model describes in a phenomenological way centroblast reaction regulation that gives rise to the development of the germinal center into a compartmentalized microenvironment. We considered centroblast proliferation and differentiation as time-dependent processes where the differentiation was increased on the cost of proliferation in the course of time. In this way we mimicked regulation mechanisms that are still unknown today, such as hypothetic signal molecules [11]. Our simulations have shown that the development of the germinal center morphology is in agreement with experimental observations. At the same time our approach offers the freedom to incorporate mechanisms like chemotaxis [12] by adjusting the time dependence of the reaction rates; however, this is left for future research.

We modeled centroblast hypermutation in terms of jumps between a one-dimensional configuration of affinity classes, which may be considered as the most simple realization of the shape-space concept [21]. The reaction rate for the interaction between centrocytes and antigen depends on their af-

finity. This induces a local winner-takes-all mechanism, where centrocytes surrounding the same antigen presenting site compete for the survival signal and the mutant with highest affinity will be most likely to reach this goal first. This local winner-takes-all mechanism gives rise to a global all-or-none behavior. Our numerical results reveal the strong selection for highest-affinity mutants and the experimentally observed all-or-none behavior as a function of the maximal mutation distance. Even though our realization of shape space is by far more simple than that in other models [11,12], our simulations confirm quantitatively the crossover in the all-or-none behavior as a function of the maximal mutation distances around $N_d=6$ to 7. For smaller values of N_d germinal centers are dominated by output cells of high affinity, while for larger values of N_d they contain no high-affinity output cells at all. In the present study we started the germinal center reactions with a germline affinity that was the same for all initial B cells. This condition may be relaxed by considering some affinity distribution for the initial B cells. Furthermore, affinity maturation may be studied as a function of the probability for affinity-lowering (p_-) and affinity-improving (p_+) mutations or including the possibility of randomly generated mutants that completely lose their ability to bind to antigen.

In our model the interaction between centrocytes and T cells is explicitly taken into account. This enabled us to study the hypothesis of centrocyte-centroblast recycling [3,28] by comparing recycling that involves centrocytes, which have received (i) both survival signals from interactions with antigen and T cells, (ii) the first survival signal from interaction with antigen only, and (iii) at least the first survival signal. Our numerical results indicate that affinity maturation is optimized by recycling involving centrocytes that have received only the first survival signal from interaction with antigen. In other words, recycling seems to improve the affinity maturation of output cells by taking the pathway that is the shortest and available at earliest times in the simulation. However, a general side effect of recycling is the decrease in the number of output cells that can eventually be so strong that the efficiency of recycling may be questioned. This would be different if one could extend the recycling hypothesis by the assumption that recycled centrocytes are for some unknown reason not again subjected to apoptosis. It would be interesting to investigate the effects on affinity maturation and on the termination of the germinal center reaction in this case. In the present paper we also restricted the study of recycling to systems with a fixed number of $N_a=7$ affinity classes. An obvious next step is the comparison of systems with different numbers of affinity classes, which is left to future research.

We finally note that the simulation methods applied in this paper are applicable to a wide range of biological systems that can be formulated in terms of reaction-diffusion models. Even though important processes in biological systems are quite often not yet fully understood, the present work illustrates that stochastic discrete event simulations are worth the effort. To be more specific, the recycling hypothesis has previously been implemented for a specific recycling pathway in various deterministic continuum models. However, our stochastic discrete event simulations indicate that affinity maturation is optimized by a different recycling pathway, which has previously not been considered. This new insight may be used to reconstruct deterministic continuum models in order to obtain qualitatively correct results and to benefit from their computational advantages over the stochastic discrete approach. We believe that using the results obtained from stochastic discrete event simulations to build deterministic continuum models will be a fruitful combination for future research.

ACKNOWLEDGMENTS

The author gratefully acknowledges lively and stimulating discussions with N. J. Figge. This work is partially supported by the Dutch "Stichting Nationale Computer Faciliteiten" (NCF) and the "Nederlandse Organisatie voor Wetenschappelijk Onderzoek" (NWO).

[1] For a general textbook on immunology see I. Roitt, J. Brostoff, and D. Male, *Immunology*, 5th ed. (Mosby International, London, 2000).
[2] For reviews on germinal centers see I. C. M. MacLennan, Annu. Rev. Immunol. **12**, 117 (1994); K. L. Wolniak, S. M. Shinall, and T. J. Waldschmidt, Crit. Rev. Immunol. **24**, 39 (2004).
[3] T. B. Kepler and A. S. Perelson, Immunol. Today **14**, 412 (1993).
[4] M. Oprea and A. S. Perelson, J. Immunol. **158**, 5155 (1997).
[5] A. Rundell, R. DeCarlo, H. HogenEsch, and P. Doerschuk, J. Theor. Biol. **194**, 341 (1998).
[6] C. Kesmir and R. J. De Boer, J. Immunol. **163**, 2463 (1999).
[7] M. Meyer-Hermann, A. Deutsch, and M. Or-Guil, J. Theor. Biol. **201**, 265 (2001).
[8] D. Iber and P. K. Maini, J. Theor. Biol. **219**, 153 (2002).
[9] M. D. Rademacher, G. Kelsoe, and T. B. Kepler, Immunol. Cell Biol. **76**, 373 (1998).
[10] S. H. Kleinstein and J. P. Singh, Int. Immunol. **15**, 871 (2003).
[11] M. Meyer-Hermann, J. Theor. Biol. **216**, 273 (2002).
[12] T. Beyer, M. Meyer-Hermann, and G. Soff, Int. Immunol. **14**, 1369 (2002).
[13] C. Kesmir and R. J. De Boer, J. Theor. Biol. **222**, 9 (2003).
[14] A well-known quote by Albert Einstein (1879–1955).
[15] D. T. Gillespie, J. Phys. Chem. **81**, 2340 (1977).
[16] D. T. Gillespie, J. Comput. Phys. **22**, 403 (1976).
[17] M. Gibson and J. Bruck, J. Phys. Chem. **104**, 1876 (2000).
[18] J. J. Lukkien, J. P. L. Segers, P. A. J. Hilbers, R. J. Gelten, and A. P. J. Jansen, Phys. Rev. E **58**, 2598 (1998).
[19] J. K. Percus, O. E. Percus, and A. S. Perelson, Proc. Natl. Acad. Sci. U.S.A. **90**, 1691 (1993).
[20] M. T. Figge, Phys. Rev. E **66**, 061901 (2002).
[21] A. S. Perelson and G. F. Oster, J. Theor. Biol. **81**, 645 (1997).
[22] M. Meyer-Hermann and T. Beyer, Dev. Immunol. (Taylor

Francis) **9**, 203 (2002).
[23] K. Hollowood and J. R. Goodlad, J. Pathol. **185**, 229 (1998).
[24] A. S. Freedman, J. M. Munro, K. Rhynhart, P. Schow, J. Daley, N. Lee, J. Svahn, L. Eliseo, and L. M. Nadler, Blood **80**, 1284 (1992).
[25] M. H. Kosco-Vilbois, H. Zentgraf, J. Gerdes, and J. Y. Bonnefoy, Immunol. Today **18**, 225 (1997).
[26] Y. J. Liu, J. Zhang, P. J. Lane, E. Y. Chan, and I. C. MacLennan, Eur. J. Immunol. **21**, 2951 (1991).
[27] S. A. Camacho, M. H. Kosco-Vilbois, and C. Berek, Immunol. Today **19**, 511 (1998).
[28] S. Han, K. Hathcock, B. Zheng, T. B. Kepler, R. Hodes, and G. Kelsoe, J. Immunol. **155**, 556 (1995).
[29] J. P. L. Segers, Ph.D. dissertation, Eindhoven University of Technology, 1998.
[30] M. Gibson, Ph.D. dissertation, California Institute of Technology, 2000.
[31] For a general textbook see B. Chopard and M. Droz, *Cellular Automata Modeling of Physical Systems* (University Press, Cambridge, England, 1998).
[32] E. Lindhout, A. Lakeman, and C. de Groot, J. Exp. Med. **181**, 1985 (1995).
[33] M. van Eijk and C. de Groot, J. Immunol. **163**, 2478 (1999).
[34] G. Kelsoe, Semin Immunol. **8**, 179 (1996).
[35] Y. J. Liu, C. Barthelemy, O. de Bouteiller, and J. Banchereau, Adv. Exp. Med. Biol. **355**, 213 (1994).
[36] J. J. Cohen, R. C. Duke, V. A. Fadok, and K. S. Sellins, Adv. Exp. Med. Biol. **10**, 267 (1992).
[37] J. G. Tew and T. E. Mandel, Immunology **37**, 69 (1979).
[38] J. Jacob, R. Kassier, and G. Kelsoe, J. Exp. Med. **173**, 1165 (1991).
[39] K. Hollowood and J. Macartney, J. Immunol. **22**, 261 (1992).
[40] G. O. Grouard, J. De Bouteiller, and Y. J. Liu, J. Immunol. **155**, 3345 (1995).
[41] F. G. Kroese, A. S. Wubbena, H. G. Seijen, and P. Nieuwenhuis, Eur. J. Immunol. **17**, 1069 (1987).
[42] M. McHeyzer-Williams, M. McLean, G. Nossal, and P. Lalor, Immunol. Cell Biol. **70**, 119 (1992).
[43] R. Skalak and S. Chien, *Handbook of Bioengineering* (McGraw-Hill, New York, 1987).
[44] R. Küppers, M. Zhao, M. L. Hansmann, and K. Rajewsky, EMBO J. **12**, 4955 (1993).
[45] G. J. Wedemayer, P. A. Patten, L. H. Wang, P. G. Schultz, and R. C. Stevens, Science **276**, 1665 (1997).
[46] C. Berek, A. Berger, and M. Apel, Cell **67**, 1121 (1991).
[47] V. M. Lentz and T. Manser, J. Immunol. **167**, 15 (2001).
[48] M. Meyer-Hermann and T. Beyer, Bull. Math. Biol. **66**, 125 (2004).